THE ASTROPHYSICAL JOURNAL, 448:954–962, 1995 August 1

NONLINEAR ENERGY TRANSFER IN SOLAR MAGNETIC LOOPS

DANIEL O. GÓMEZ
Departamento de Física, Facultad de Ciencias Exactas y Naturales, Universidad de Buenos Aires, (1428) Buenos Aires, Argentina
EDWARD E. DELUCA
Harvard-Smithsonian Center for Astrophysics, 60 Garden Street, Cambridge, MA 02138
AND
ALEXANDER N. MCCLYMONT
Institute for Astronomy, University of Hawaii, 2680 Woodlawn Drive, Honolulu, HI 96822
Received 1994 April 28; accepted 1995 January 17

ABSTRACT

Active region coronal loops are widely believed to be heated by ohmic dissipation of field-aligned electric currents. These currents are driven by turbulent photospheric motions which twist and shear the magnetic footpoints of loops. Fine-scale structure in the corona is required in order to dissipate the currents rapidly enough to account for coronal heating. A long-standing controversy surrounds the question: is the fine-scale filamentation the result of magnetohydrodynamic (MHD) instabilities, or of dynamical nonequilibrium, or is it merely the direct product of the turbulent footpoint motions themselves? We present a simple model for the evolution of the coronal magnetic field, with no fine-scale structure in the imposed footpoint motions. The model consists of a three-mode truncation of the "reduced" MHD equations. One mode is driven by a stationary velocity field at the footpoints; the other two modes, of different spatial frequencies, are amplified through interaction with the driven mode. After approximately one photospheric turnover time, the coronal field loses equilibrium, and evolves rapidly to a new configuration, transferring energy to the two nondriven modes. The timescale of rapid nonequilibrium evolution is $(\tau_A \tau_p)^{1/2}$, where τ_A is the Alfvén transit time along the loop and τ_p is the photospheric turnover time. Regarding this simple model as a building block of a much more complex process, we see that dynamical nonequilibrium should be able to produce a cascade of free energy to fine spatial scales where it can be dissipated rapidly enough to account for coronal heating, as envisioned by Parker.

Subject headings: instabilities — MHD — Sun: corona — Sun: magnetic fields

1. INTRODUCTION

Soft X-ray observations of the solar corona performed over the last few decades consistently reveal a highly structured brightness distribution, which is believed to be a consequence of the presence of magnetic fields confining the X-ray emitting plasma and governing its dynamics (Vaiana & Rosner 1978). More recently, the Normal Incidence X-ray Telescope (NIXT) has yielded subarcsecond images of the solar corona in a series of successful rocket flights. These observations show coronal loops with a highly filamentary internal structure, down to the resolution limit of the instrument (Golub et al. 1990).

The source of energy for coronal heating almost certainly lies in photospheric convective motions: the question is how is the energy transferred. Both acoustic coupling through the generation and dissipation of shock waves, and the transfer of energy by magnetic stresses, have been investigated in numerous studies. The fact that the strongest heating is found in active regions suggests a coupling between convective motions and the magnetic field, although it could be argued that the role of the magnetic field is solely to contain the high-pressure heated gas. Even though the subphotospheric velocity field apparently provides enough input to compensate for the conductive and radiative losses of the coronal plasma, the precise dissipation mechanism is still uncertain. The most natural candidate is Joule dissipation, but the typical timescale to dissipate coronal magnetic stresses on the length scale of the driving photospheric granule motions is exceedingly long. Therefore, most of the current theories of coronal heating deal with different mechanisms to speed up Joule dissipation (see Narain & Ulmschneider 1990 or Gómez 1990 for recent reviews).

The formation of small-scale current-carrying structures in coronal loops is necessary to enhance magnetic energy dissipation to provide for the heating of the confined plasma. Parker (1972, 1983) proposes that footpoint motions of coronal loops continuously drive the magnetic field into states of dynamical nonequilibrium in which tangential discontinuities spontaneously form. Parker asserts that the magnetic reconnection taking place in this stochastic distribution of current sheets both enhances the ohmic dissipation of magnetic energy and simplifies the stressed magnetic structures (topological dissipation). Van Ballegooijen (1986) presented a quasi-static force-free model displaying the development of an energy cascade from large to small length scales as a result of random motions imposed at the photospheric boundaries. Mikić, Schnack, & van Hoven (1989) solve the time-dependent magnetohydrodynamic (MHD) equations with viscosity, following a sequence of excitation-relaxation steps. They find that the system relaxes to equilibria which agree with those computed by van Ballegooijen and confirm the presence of an energy cascade process. More recently, Longcope & Sudan (1992) reported that the quasi-static evolution of coronal loops driven by slow footpoint motions are likely to undergo sudden "losses of equilibrium," at which time the system departs from a force-free configuration and evolves in a rather dynamic fashion. Furthermore, they show the formation of highly structured electric currents associated with the development of these

quasi-static crises. It is interesting to note that in spite of the obvious differences between these models, they share in common the development of small-scale dissipative structures as a way to enhance Joule dissipation.

The formation of new spatial structure is a manifestation of the nonlinear behavior of the dynamics of coronal loops. In the present paper, we analyze in detail the generation of new spatial patterns in a coronal loop driven by footpoint motions. We restrict our analysis to a very simple model of a coronal loop, which nonetheless shows the development of nonlinear rapid transients leading to the growth of new patterns inside the corona. We use a truncated version of the reduced MHD (RMHD) equations, consisting of a resonant triad of three Fourier modes. One of the modes is externally driven by a stationary pattern of footpoint motions. This single Fourier mode pattern is intended to simulate granular photospheric motions. The initial effect of this driving action is simply to bend the loop field lines, following the spatial pattern imposed at the photospheric boundaries. However, on timescales on the order of one photospheric turnover time, this structure is found to undergo a loss of equilibrium, leading very efficiently to the development of new spatial structure, described in our simple model by the superposition of three Fourier modes, two of which have received no contribution from the flow motions imposed at the photospheric ends. The rapid "nonequilibrium" evolution involves a net energy transfer from the externally driven mode to the two new modes. An appreciable fraction of the total energy in the system remains in the new modes when a new quasi-steady state is reached. Once the three modes share comparable amounts of energy, each of them is free to interact with new triads, and therefore the three-mode truncation becomes invalid.

Because of the simplicity of our model, we do not expect our results to be directly comparable to observations of the dynamics of coronal loops. The aim of the present paper is rather to point out the existence and efficiency of these nonlinear interactions in generating new spatial structure in the interior of coronal loops, regarding them as building blocks of a much more complex dynamical process. In § 2 we introduce the RMHD equations to be used in our analysis, and in § 3 we describe the truncation to three Fourier modes. In § 4 we assume that the footpoint motions are sufficiently slow to allow the system to evolve through a sequence of quasi-static, force-free equilibria. We find that after timescales of the order of the turnover time, this equilibrium is suddenly lost and the system enters a more dynamic stage. As detailed in § 5, the linear regime of this dynamic stage, after the force-free equilibrium is lost, is governed by a timescale which is the geometric average between the turnover time and the Alfvén time (travel time of an Alfvén wave through the loop). In § 5 we also present the results of a numerical integration of the truncated RMHD equations. The main features of this nonlinear dynamical system are summarized in § 6. Finally, in § 7 we discuss the possible implications of these results for the coronal heating problem.

2. REDUCED MAGNETOHYDRODYNAMIC EQUATIONS

We consider a coronal loop of length L with a cross section $D \times D$. We discard toroidal effects because $D \ll L$. The main magnetic field is assumed to be uniform and parallel to the axis of the loop, $\boldsymbol{B}_0 = B_0 \hat{z}$. The planes $z = 0$ and $z = L$ correspond to the loop footpoints at the solar photosphere. Assuming that the size scale of footpoint motions is much smaller than L, then we are able to use the "reduced MHD" (RMHD) approximation (Strauss 1976), in which the plasma moves incompressibly in planes perpendicular to the axial field $\boldsymbol{B}_0$, and the transverse component of the magnetic field is small compared to B_0. We also assume that the gas pressure is much smaller than the magnetic pressure in the coronal part of the loop, and rises discontinuously to a large value at the photospheric plates. This disparity between the photospheric and coronal plasmas, combined with their very high electric conductivities, allow photospheric convective motions to easily drive magnetic stresses in the corona (Parker 1972).

For consistency with the RMHD approximation, we take the motions in the photospheric endplates to be incompressible. The photospheric motions generate transverse components of velocity ($\boldsymbol{u}$) and magnetic field ($\boldsymbol{b}$) in the corona. Expressing the magnetic field strength in terms of the Alfvén velocity [$\boldsymbol{B} \rightarrow \boldsymbol{B}/(4\pi\rho)^{1/2}$; ρ is the constant density], we have

$$\boldsymbol{B} = v_A \hat{z} + \boldsymbol{b}(x, y, z, t), \quad \boldsymbol{b} \cdot \hat{z} = 0, \tag{1}$$

$$\boldsymbol{u} = \boldsymbol{u}(x, y, z, t), \quad \boldsymbol{u} \cdot \hat{z} = 0, \tag{2}$$

where $v_A = B_0(4\pi\rho)^{-1/2}$ is the Alfvén velocity of the plasma (ρ: mass density). Since both $\boldsymbol{b}$ and $\boldsymbol{u}$ are two-dimensional and divergence-free fields, they can be represented by scalar potentials

$$\boldsymbol{b} = \nabla \times (a\hat{z}) = \nabla a(x, y, z, t) \times \hat{z}, \tag{3}$$

$$\boldsymbol{u} = \nabla \times (\varphi\hat{z}) = \nabla\varphi(x, y, z, t) \times \hat{z}. \tag{4}$$

Hereafter, the operator ∇ is reserved to indicate derivatives in the (x, y) plane, while derivatives along the z-direction are written explicitly.

The magnetohydrodynamic (MHD) equations for the potentials φ and a under the assumptions listed above, are

$$\partial_t a = v_A \partial_z \varphi + [\varphi, a] + \eta\nabla^2 a, \tag{5}$$

$$\partial_t \omega = v_A \partial_z j + [\varphi, \omega] - [a, j] + \nu\nabla^2\omega, \tag{6}$$

where

$$\omega = -\nabla^2\varphi, \quad j = -\nabla^2 a, \tag{7}$$

and the Poisson brackets are defined as

$$[A, B] = \hat{z} \cdot \nabla A \times \nabla B = \partial_x A \partial_y B - \partial_y A \partial_x B. \tag{8}$$

These equations are usually referred to as the *reduced* MHD equations (Strauss 1976). Equation (5) describes the advection of the potential a, and equation (6) corresponds to the evolution of vorticity. As boundary conditions for the coronal loop, we choose: periodic boundary conditions on the (x, y) plane, and prescribed velocity fields at both photospheric plates, $\varphi_{(z=0)}(x, y, t)$ and $\varphi_{(z=L)}(x, y, t)$. The terms $v_A \partial_z$ represent the dynamic coupling between neighboring $z = constant$ planes. The role of these terms is therefore essential to transfer energy from the footpoints into the coronal part of the loop. The ∇^2 terms in equations (5)–(6) represent dissipative effects, the constants η and ν being the resistivity and viscosity coefficients, respectively. For a typical coronal plasma these coefficients are extremely small and therefore for the truncated system, where only large scales are involved, the dissipative terms can safely be neglected. The nonlinear terms in these equations are represented by the Poisson brackets. Their role in the dynamic evolution of the system is to couple its normal modes, in such a way that energy (and other ideal invariants) can be transferred between them. In the next section we consider a truncation of three Fourier modes of the reduced MHD equations, and show

how their nonlinear interaction can efficiently excite new modes in the corona which are not being externally driven from the photosphere.

3. TRUNCATED SYSTEM OF THREE FOURIER MODES

Let us consider the case of stationary footpoint motions. In this case, the functions $\varphi_{(z=0)}$ and $\varphi_{(z=L)}$ are independent of time. Since we are assuming periodic boundary conditions in the transverse directions of equations (5)–(8), the corresponding normal modes are spatial Fourier modes whose amplitudes depend on height and time,

$$a(x, y, z, t) = \sum_{\boldsymbol{k}} a_{\boldsymbol{k}}(z, t) e^{i\boldsymbol{k}\cdot\boldsymbol{x}}, \quad a_{-\boldsymbol{k}} = a_{\boldsymbol{k}}^{*}, \tag{9}$$

$$\varphi(x, y, z, t) = \sum_{\boldsymbol{k}} \varphi_{\boldsymbol{k}}(z, t) e^{i\boldsymbol{k}\cdot\boldsymbol{x}}, \quad \varphi_{-\boldsymbol{k}} = \varphi_{\boldsymbol{k}}^{*}. \tag{10}$$

If no-slip boundary conditions are enforced at $z = 0, L$, the amplitudes $a_{\boldsymbol{k}}$ and $\varphi_{\boldsymbol{k}}$ can be expressed as a linear combination of two different types of solutions: DC-type solutions

$$\varphi_{\boldsymbol{k}}^{\mathrm{DC}} \simeq \varphi_{\boldsymbol{k}}(z = 0) + \frac{z}{L}\left[\varphi_{\boldsymbol{k}}(z = L) - \varphi_{\boldsymbol{k}}(z = 0)\right], \tag{11}$$

$$a_{\boldsymbol{k}}^{\mathrm{DC}} \simeq \frac{t}{\tau_{\mathrm{A}}}\left[\varphi_{\boldsymbol{k}}(z = L) - \varphi_{\boldsymbol{k}}(z = 0)\right], \tag{12}$$

and AC-type solutions,

$$\varphi_{\boldsymbol{k}}^{\mathrm{AC}} \simeq \sum_{l=1}^{\infty} C_l \sin\left(\frac{\pi l z}{L}\right)\cos\left(\frac{\pi t}{\tau_{\mathrm{A}}}\right), \tag{13}$$

$$a_{\boldsymbol{k}}^{\mathrm{AC}} \simeq \sum_{l=1}^{\infty} C_l \cos\left(\frac{\pi l z}{L}\right)\sin\left(\frac{\pi t}{\tau_{\mathrm{A}}}\right). \tag{14}$$

The possibility of pumping traveling Alfvén waves is not present in our analysis, because we are considering stationary footpoint motions. DC-type solutions ($\varphi_{\boldsymbol{k}}^{\mathrm{DC}}$, $a_{\boldsymbol{k}}^{\mathrm{DC}}$) can only be excited by footpoint motions which contain the mode $\boldsymbol{k}$ in their convective pattern [$\varphi_{\boldsymbol{k}}(z = L) \neq 0$]. On the other hand, AC-type solutions correspond to stationary Alfvén waves, with velocity nodes at $z = 0, L$. The amplitude C_l is completely unrelated to footpoint motions and can only arise from nonlinear interaction with other Fourier modes. The main goal of this paper is to show that nonlinear mode coupling is indeed an efficient mechanism for exciting new modes (and therefore generating magnetic structure) in the corona.

To analyze the nonlinear coupling between modes in detail, we concentrate on a truncated version of the real problem: a set of three Fourier modes. Because of the quadratic form of all nonlinear terms in equations (5)–(6), each Fourier mode $\boldsymbol{k}_0$ couples with pairs of modes $\boldsymbol{k}_1$, $\boldsymbol{k}_2$ satisfying the rule $\boldsymbol{k}_2 = \boldsymbol{k}_0 + \boldsymbol{k}_1$. Resonantly coupled triads are the dominant nonlinear interaction in many physical systems displaying quadratic nonlinearities, and therefore a number of approximate models have been developed to predict the effects of these interactions (see, for instance Segur 1984 and Zakharov et al. 1992). The dynamic equations for the amplitudes φ_{ki}, a_{ki} of Fourier modes in a triad ($\boldsymbol{k}_0$, $\boldsymbol{k}_1$, $\boldsymbol{k}_2$), can readily be derived from the general equations (5)–(6). More specifically, we represent the scalar fields as

$$\begin{aligned}\psi(x, y, z, t) = {} & \psi_0(z, t)\cos(2\pi k_{0x} x)\cos(2\pi k_{0y} y) \\ & + \psi_1(z, t)\cos(2\pi k_{1x} x)\cos(2\pi k_{1y} y) \\ & + \psi_2(z, t)\sin(2\pi k_{2x} x)\sin(2\pi k_{2y} y),\end{aligned} \tag{15}$$

where ψ is either φ or a, and the $\psi_i (i = 0, 1, 2)$ are real valued amplitudes. This expresion corresponds to an expansion in terms of even functions on the plane (x, y), whose wavenumber labels satisfy the rule $\boldsymbol{k}_2 = \boldsymbol{k}_0 + \boldsymbol{k}_1$. Under this approximation, all other nonlinear interactions are neglected. The dynamic equations for the three-mode system can be written in a compact form (Longcope & Sudan 1991) by defining the vectors $\boldsymbol{\Phi} = (\varphi_0, \varphi_1, \varphi_2)$ and $\boldsymbol{A} = (a_0, a_1, a_2)$; then

$$\partial_t \boldsymbol{A} = \partial_z \boldsymbol{\Phi} + \boldsymbol{\Phi} \times \boldsymbol{A}, \tag{16}$$

$$\partial_t \boldsymbol{\Omega} = \partial_z \boldsymbol{J} + \boldsymbol{\Phi} \times \boldsymbol{\Omega} - \boldsymbol{A} \times \boldsymbol{J}, \tag{17}$$

where

$$\boldsymbol{\Omega} = \boldsymbol{L}\boldsymbol{\Phi}, \quad \boldsymbol{J} = \boldsymbol{L}\boldsymbol{A} \tag{18}$$

correspond to the amplitudes of vorticity and electric current, and

$$\boldsymbol{L} = \begin{pmatrix} k_0^2 & 0 & 0 \\ 0 & k_1^2 & 0 \\ 0 & 0 & k_2^2 \end{pmatrix}. \tag{19}$$

The quantities displayed in equations (16)–(19) are dimensionless. Time is in units of $\tau_{\mathrm{A}} = L/v_{\mathrm{A}}$, the position z along the loop is in units of L, the transverse scales are in units of the granule size $l = D/N_0$ (D: loop width, N_0: integer), and the scalar fields $\boldsymbol{\Phi}$ and $\boldsymbol{A}$ are in units of $l^2/(\pi^2\gamma\tau_{\mathrm{A}})$. The constant $\gamma = (\hat{z}\cdot\boldsymbol{k}_2 \times \boldsymbol{k}_1)$ is related to the geometric structure of the triad. We must complement equations (16)–(17) with an adequate set of initial and boundary conditions. In § 5 we solve these equations for the following boundary conditions:

$$\varphi_{0,1,2}(0, t) = 0, \tag{20}$$

$$\varphi_0(1, t) = \varphi_0 = \text{constant}, \quad \varphi_{1,2}(1, t) = 0, \tag{21}$$

while the initial conditions are

$$\varphi_0(z, 0) = \varphi_0 z, \quad \varphi_{1,2}(z, 0) \simeq 0, \tag{22}$$

$$a_{0,1,2} \simeq 0. \tag{23}$$

The underlying idea for this choice is to simulate the external driving of just one mode ($\boldsymbol{k}_0$) by a stationary photospheric motion, and see whether any excitation of modes $\boldsymbol{k}_1$, $\boldsymbol{k}_2$, takes place as a result of their nonlinear coupling.

4. FORCE-FREE SOLUTIONS AND LOSS OF EQUILIBRIUM

The expression describing static ($\varphi = 0$) ideal ($v = 0$) equilibria in equation (6) corresponds to the requirement that the Lorentz force is curl-free [$\nabla \times (\boldsymbol{J} \times \boldsymbol{B}) = 0$], which comprises force-free equilibria ($\boldsymbol{J} \times \boldsymbol{B} = 0$) as particular cases. However, hereafter we will simply use term "force-free" when referring to these equilibria. Since photospheric motions typically occur on timescales $\tau_p = l/u_p \approx 10^3$ s, much longer than the Alfvén time $\tau_{\mathrm{A}} = L/v_{\mathrm{A}} \approx 10$ s, coronal loops are likely to be close to a force-free equilibrium. More specifically, coronal loops are often assumed to follow a continuous sequence of force-free equilibria at the slow timescale τ_p (van Ballegooijen 1985; Longcope & Sudan 1992). Under this additional assumption, equations (16)–(17) for our truncated system of three modes become

$$\partial_t \boldsymbol{A} = \partial_z \boldsymbol{\Phi} + \boldsymbol{\Phi} \times \boldsymbol{A}, \tag{24}$$

$$0 = \partial_z \boldsymbol{J} - \boldsymbol{A} \times \boldsymbol{J}. \tag{25}$$

Equation (25) describes the aforementioned equilibrium and is formally analogous to the two-dimensional Euler equation for an inviscid flow, where z plays the role of time and $\boldsymbol{J}$ is the vorticity. Equation (24) describes the advection of the magnetic field by the plasma and hence the evolution of the system as it slowly and continuously changes from one force-free equilibrium to the next.

The implicit assumption here is that there is always a neighboring force-free equilibrium available, so that the system can evolve without leaving the force-free manifold that is embedded in the space of solutions of the general equations (16)–(17). However, the failure of the RMHD equations to quasi-statically follow force-free equilibria under certain circumstances has recently been reported by Longcope & Sudan (1992). When this "loss of equilibrium" occurs, the system seeks to relax to a new equilibrium branch at the fast τ_A timescale, which is completely absent in the evolution described by equations (24)–(25). Below we show how this loss of equilibrium takes place in the three-mode system.

We assume that the triad is dominated by the externally driven mode $\boldsymbol{k}_0$, which as a result displays a DC-type solution (see eqs. [11]–[12]). After linearizing equation (25) we obtain

$$\partial_z \begin{pmatrix} A_1 \\ A_2 \end{pmatrix} = -\varphi_0 t \begin{pmatrix} 0 & r_1 \\ r_2 & 0 \end{pmatrix} \begin{pmatrix} A_1 \\ A_2 \end{pmatrix}, \tag{26}$$

where $r_1 = (k_2^2 - k_0^2)/k_1^2$ and $r_2 = (k_0^2 - k_1^2)/k_2^2$ are constant coefficients. The corresponding solutions are

$$A_1(z, t) = -r_1 (C e^{\Lambda z t} + C' e^{-\Lambda z t}), \tag{27}$$

$$A_2(z, t) = \sqrt{r_1 r_2} (C e^{\Lambda z t} - C' e^{-\Lambda z t}), \tag{28}$$

where $\Lambda = \varphi_0 (r_1 r_2)^{1/2}$ and the coefficients $C(t)$ and $C'(t)$ are arbitrary functions of time, to be determined after substituting equations (27)–(28) into the linearized version of equation (24),

$$\left[\partial_z + \varphi_0 t \begin{pmatrix} 0 & 1 \\ -1 & 0 \end{pmatrix} \right] \begin{pmatrix} \varphi_1 \\ \varphi_2 \end{pmatrix} = \varphi_0 z \begin{pmatrix} 0 & 1 - r_1 \\ -1 - r_2 & 0 \end{pmatrix} \begin{pmatrix} A_1 \\ A_2 \end{pmatrix} + \begin{pmatrix} \hat{A}_1 \\ \hat{A}_2 \end{pmatrix}, \tag{29}$$

where $\hat{A}_{1,2}$ are equivalent to expressions (27)–(28), but with coefficients $\dot{C}$, $\dot{C}'$. Hereafter the upper dot indicates time derivative. The general solution to the inhomogeneous equation (29) is

$$\varphi_1(z, t) = (D e^{i\varphi_0 z t} + D' e^{-i\varphi_0 z t}) + \frac{z}{t} A_1 + \frac{r_1 + 1}{(1 + r_1 r_2)\varphi_0 t} \left(\frac{A_2}{t} - \hat{A}_2 \right), \tag{30}$$

$$\varphi_2(z, t) = -i(D e^{i\varphi_0 z t} - D' e^{-i\varphi_0 z t}) + \frac{z}{t} A_2 + \frac{r_2 - 1}{(1 + r_1 r_2)\varphi_0 t} \left(\frac{A_1}{t} - \hat{A}_1 \right). \tag{31}$$

By enforcing no-slip boundary conditions on φ_1, φ_2 at both $z = 0$ and $z = 1$, we obtain four ODEs to determine C, C', D, D' as a function of time. From $\varphi_{1,2}(0, t) = 0$ we obtain

$$D = \frac{R_1}{2\varphi_0 t} \left(\dot{C} - \dot{C}' - \frac{C - C'}{t} \right) - \frac{i R_2}{2\varphi_0 t} \left(\dot{C} + \dot{C}' - \frac{C + C'}{t} \right), \tag{32}$$

$$D' = \frac{R_1}{2\varphi_0 t} \left(\dot{C} - \dot{C}' - \frac{C - C'}{t} \right) + \frac{i R_2}{2\varphi_0 t} \left(\dot{C} + \dot{C}' - \frac{C + C'}{t} \right), \tag{33}$$

where $R_1 = (r_1 r_2)^{1/2}(r_1 + 1)/(1 + r_1 r_2)$ and $R_2 = r_1(r_2 - 1)/(1 + r_1 r_2)$. Using $\varphi_{1,2}(1, t) = 0$, and substituting equations (32) and (33) in (30) and (31), we obtain

$$\boldsymbol{M} \begin{pmatrix} \dot{C} \\ \dot{C}' \end{pmatrix} = \boldsymbol{M}' \begin{pmatrix} C \\ C' \end{pmatrix}, \tag{34}$$

where

$$\boldsymbol{M}(t) = \frac{1}{\varphi_0 t} \begin{bmatrix} x_{11} & x_{12} \\ x_{21} & x_{22} \end{bmatrix}, \tag{35}$$

where $x_{11} = R_1 \cos(\varphi_0 t) + R_2 \sin(\varphi_0 t) - R_1 e^{\Lambda t}$, $x_{12} = -R_1 \cos(\varphi_0 t) + R_2 \sin(\varphi_0 t) + R_1 e^{-\Lambda t}$, $x_{21} = R_1 \sin(\varphi_0 t) - R_2 \cos(\varphi_0 t) + R_2 e^{\Lambda t}$, and $x_{22} = -R_1 \sin(\varphi_0 t) - R_2 \cos(\varphi_0 t) + R_2 e^{-\Lambda t}$, and

$$\boldsymbol{M}'(t) = \frac{1}{t} \boldsymbol{M}(t) + \frac{1}{t} \begin{pmatrix} r_1 e^{\Lambda t} & r_1 e^{-\Lambda t} \\ -\sqrt{r_1 r_2}\, e^{\Lambda t} & \sqrt{r_1 r_2}\, e^{-\Lambda t} \end{pmatrix}. \tag{36}$$

The matrices $\boldsymbol{M}$ and $\boldsymbol{M}'$ are regular at $t = 0$. For any given choice $C(0) = C_0$, $C'(0) = C'_0$ of the initial conditions, equation (34) can be integrated and equations (27)–(28) and (30)–(31) can be used to construct a particular force-free solution, labeled by the pair (C_0, C'_0). However, all of these solutions break down at a time $t = \tau_*$ where the matrix $\boldsymbol{M}(t)$ becomes singular (i.e., $\det[\boldsymbol{M}(\tau_*)] = 0$). We associate this breakdown of the force-free solutions with a loss of equilibrium, in the sense that the coefficients C and C' diverge on a timescale $\Delta t \approx 0$ around $t = \tau_*$. When this happens, the force-free approximation is no longer valid (eqs. [24]–[25]) and the full equations (16)–(17) must be considered, bringing the fast time scale τ_A back into play.

Since Λ is proportional to φ_0, $\boldsymbol{M}$ is a function of $\varphi_0 t$ only ($\varphi_0 t \approx t/\tau_p$), implying that the loss of equilibrium occurs when the field has been "wound up" by a certain amount, independent of the timescales τ_A and τ_p.

5. THREE-MODE NONEQUILIBRIUM

5.1. *Linear Regime*

Once force-free equilibrium is lost (see previous section), we expect the system to undergo some sort of unstable evolution, seeking a new equilibrium configuration. Starting from equations (16)–(17), we estimate a rise time which describes the global long time evolution of the new modes $\boldsymbol{k}_1$ and $\boldsymbol{k}_2$. As in the previous section, we assume the truncated system to be initially dominated by the $\boldsymbol{k}_0$ mode, whose potentials are thus simply $\varphi_0(z, t) = \varphi_0 z$ and $a_0(z, t) = \varphi_0 t$. We linearize equations (16)–(17), keeping terms up to first order in (A_1, A_2),

(φ_1, φ_2), to obtain

$$\partial_t \begin{pmatrix} A_1 \\ A_2 \end{pmatrix} = \partial_z \begin{pmatrix} \varphi_1 \\ \varphi_2 \end{pmatrix} + \begin{pmatrix} 0 & 1 \\ -1 & 0 \end{pmatrix} \left[\varphi_0 t \begin{pmatrix} \varphi_1 \\ \varphi_2 \end{pmatrix} - \varphi_0 z \begin{pmatrix} A_1 \\ A_2 \end{pmatrix} \right], \tag{37}$$

$$\partial_t \begin{pmatrix} \varphi_1 \\ \varphi_2 \end{pmatrix} = \partial_z \begin{pmatrix} A_1 \\ A_2 \end{pmatrix} + \begin{pmatrix} 0 & r_1 \\ r_2 & 0 \end{pmatrix} \left[\varphi_0 t \begin{pmatrix} A_1 \\ A_2 \end{pmatrix} - \varphi_0 z \begin{pmatrix} \varphi_1 \\ \varphi_2 \end{pmatrix} \right]. \tag{38}$$

For times longer than the Alfvén timescale ($t \gg 1$), the leading terms on the right-hand sides of equations (37)–(38) are those proportional to $\varphi_0 t$. Neglecting the remaining terms, equations (37)–(38) can readily be integrated and a global rise time can be estimated. The potentials for the new modes ($\boldsymbol{k}_1$, $\boldsymbol{k}_2$) evolve like

$$\psi(t) \approx \exp\left(\tfrac{1}{2}\Gamma \varphi_0 t^2\right), \quad \psi = \varphi_{1,2}, a_{1,2}, \tag{39}$$

where the real parts of

$$\Gamma_1^{\pm} = \pm\sqrt{-r_1}, \quad \Gamma_2^{\pm} = \pm\sqrt{r_2}, \tag{40}$$

define the (dimensionless) nonequilibrium evolution rates.

In dimensional form, equations (39)–(40) estimate a nonequilibrium rise time which scales like $\tau_{\rm rise} \approx (\tau_A \tau_p)^{1/2}$ multiplied by a constant coefficient which depends on the triad (i.e., on r_1 and r_2). This means that, globally, modes $\boldsymbol{k}_1$ and $\boldsymbol{k}_2$ grow on a timescale which is intermediate between the fast (τ_A) and slow (τ_p) timescales of the problem. Therefore, our original assumption of concentrating on the long-term evolution ($t \gg \tau_A$) seems justified.

In the following subsection we numerically integrate the nonlinear equations (16)–(17) and confirm that the scaling for the rise time is indeed correct. We also analyze the saturation of the phase of rapid nonequilibrium evolution.

5.2. *Nonlinear Saturation*

We integrated equations (16)–(17) numerically, with the boundary and initial conditions corresponding to the situation of externally driving one single Fourier mode through the stationary motion of one of the footpoints (eqs. [20]–[23]). The equations were advanced in time using a second-order implicit method, with a staggered z-grid for potentials $\boldsymbol{\Phi}$ and $\boldsymbol{A}$. Boundary conditions for the velocity potential $\boldsymbol{\Phi}$ were enforced at $z = 0$ and $z = L$ (eqs. [20]–[21]).

We tested the accuracy of the code by checking the conservation of the ideal invariants (energy, squared vector potential, and cross-helicity; see Gómez 1990 for a detailed description of these conservation laws). We find that these conservation laws are satisfied with an accuracy better than 99%.

So far we have not specified any particular triad, or set of three modes. In order to see which triads are more efficient in transferring energy from the externally driven mode $\boldsymbol{k}_0$ to the new modes $\boldsymbol{k}_1$ and $\boldsymbol{k}_2$, we integrated equations (16)–(17) for an array of triads in the range $0 \le k_{2x} \le 2k_0$ and $0 \le k_{2y} \le k_0$, where $\boldsymbol{k}_0 = (k_0, 0)$ and $\boldsymbol{k}_2 = \boldsymbol{k}_0 + \boldsymbol{k}_1$. In Figure 1 we show the fraction of the total energy stored in the new modes as a function of triad. The triad for which this ratio is maximum is $\boldsymbol{k}_2 = (1.2k_0, 0.9k_0)$. Hereafter all our results correspond to this particular triad. However, it is important to note that the maximum in Figure 1 is quite broad, and therefore a whole set of triads will get efficiently excited and saturate at about the same level. What this means is that before nonlinear saturation occurs, the three-mode truncation is no longer a good approximation, since by then many modes will be simultaneously absorbing energy from the externally driven mode and they will start interacting with one another.

In Figure 2 we show the total energy of the triad as a function of time, and the energy in the undriven modes as well. Time is in units of the photospheric turnover time. Before equilibrium is lost, most of the energy is stored as magnetic energy of the externally driven mode, increasing in time like $W \approx t^2$. In the linear stage, the energy of the new modes rises rather steeply, like $W_{1+2} \approx \exp[(t/\tau_{\rm rise})^2]$. In Figure 2 we have plotted $\ln(W)$ versus t^2 so that this part of the curve looks like a straight line, with a slope $\approx \tau_{\rm rise}^{-2}$. We performed several runs with different values of τ_A and τ_p and confirmed that $\tau_{\rm rise}$ indeed scales like $\tau_{\rm rise} \approx (\tau_A \tau_p)^{1/2}$, as predicted in the previous subsection. For the run displayed in Figure 2 we used $\tau_A/\tau_p = 0.1$.

In Figure 3 we show how the energy in each model distributes into kinetic and magnetic components. We see that the externally driven mode remains magnetically dominated, before and after the rapid transient. Mode $\boldsymbol{k}_2$, however, becomes an essentially kinetic mode.

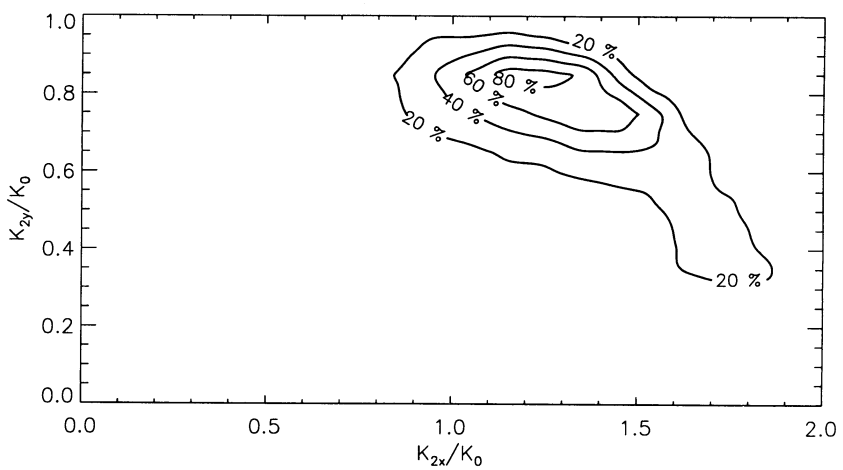

FIG. 1.—Fraction of the total energy stored in the new modes after the saturation of growth as a function of (k_{2x}, k_{2y}). The externally driven mode in this diagram is located at (1, 0).

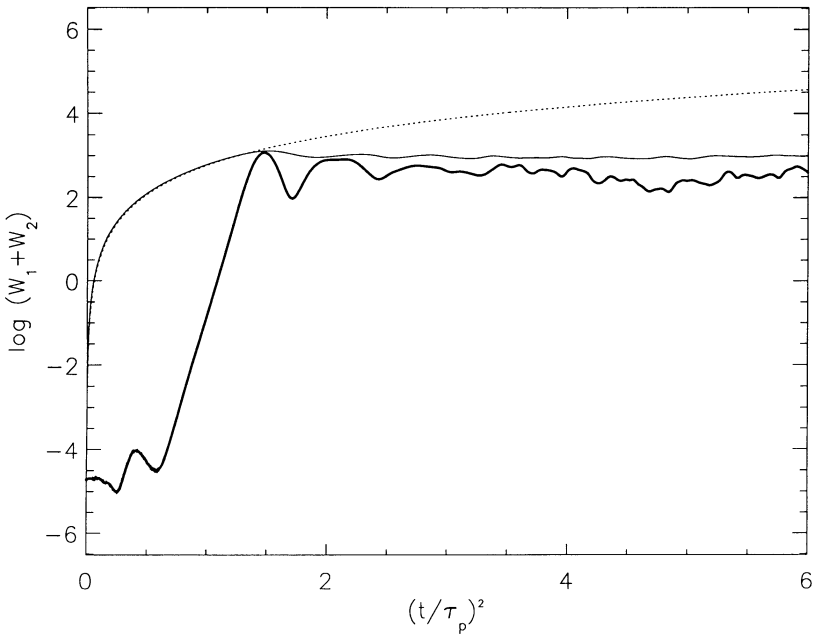

FIG. 2.—Total energy (*thin line*) and energy in the new modes (*thick line*) as a function of time for the most rapidly growing triad. The dotted line shows the law $W \approx t^2$, corresponding to total energy in the absence of nonequilibrium.

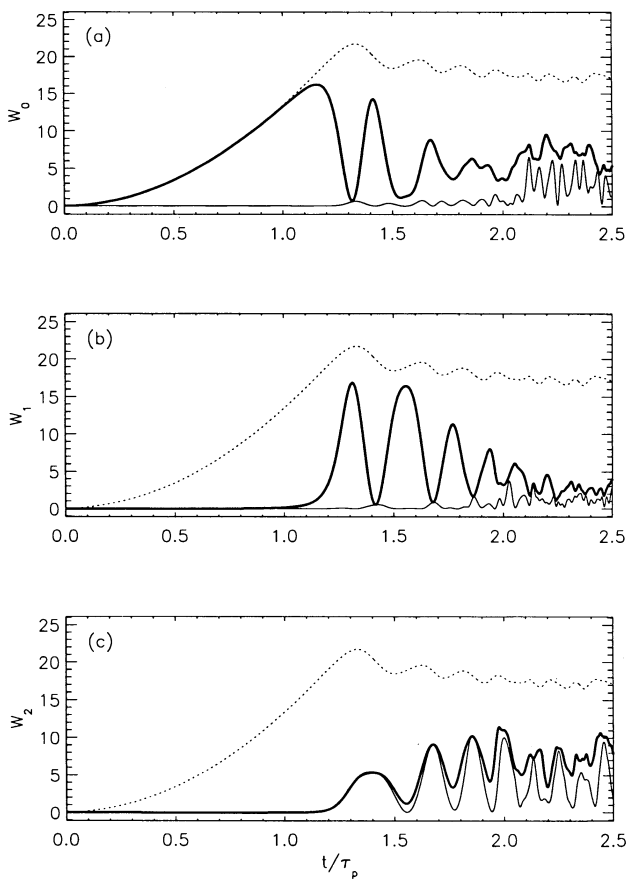

FIG. 3.—Kinetic (*thin line*) and total energy (*thick line*) per mode as a function of time. The total energy of the triad (*dotted line*) is shown for reference. (*a*) In mode k_0; (*b*) in mode k_1; (*c*) in mode k_2.

Figure 4 shows how the magnetic energy per unit length $W_B = \frac{1}{2}\boldsymbol{A} \cdot \boldsymbol{J}$ depends on z, at different times. From equation (25) we readily derive that for a force-free configuration, the total magnetic energy is independent of z. Therefore a horizontal line in Figure 4 ($\partial_z W_B \simeq 0$) is a sufficient condition for the system to be in a force-free equilibrium. We can see that this is the case before equilibrium is lost. However, during the saturation stages and after, the system is far from a force-free configuration. We note that the absence of dissipation effects in our analysis keeps the system from relaxing to a new equilibrium. The tendency of the truncated system to store an appreciable fraction of its total energy as kinetic energy will probably diminish if more modes are added.

The photospheric motion imposed at the upper boundary is described by $\varphi(x, y, z = 1) = \varphi_0 \cos(2\pi k_{0x} x) \cos(2\pi k_0 y)$, which is a stationary flow represented by just one Fourier mode, $\boldsymbol{k}_0 = [\frac{1}{2}, \frac{1}{2}]$. The corresponding spatial pattern consists of square cells of linear size $l \approx k_0^{-1}$. Since the circulation time is different on different streamlines, we define τ_p as the turnover time of a streamline at half-radius. The fluid in the innermost streamlines describes more or less circular trajectories with periods shorter than τ_p ($\approx \tau_p/2$ toward the center), while the outermost fluid moves along squarish streamlines with periods longer than τ_p (the period diverges toward the cell walls). Time in all our figures is in units of the photospheric turnover time τ_p.

In Figure 5 we display a time sequence of contour plots of the stream function $\varphi(x, y, z = \frac{1}{2})$, in a loop section at $z = \frac{1}{2}$. The solid-line contours correspond to anti-clockwise motions and the dotted contours to clockwise flows. For reference, we overlay the square grid corresponding to the cell walls at the photosphere. Before nonequilibrium sets in, the stream function displays the flow pattern imposed in the upper photospheric plate (the lower plate remains at rest). While the rapid evolution is developing, this pattern distorts more and more.

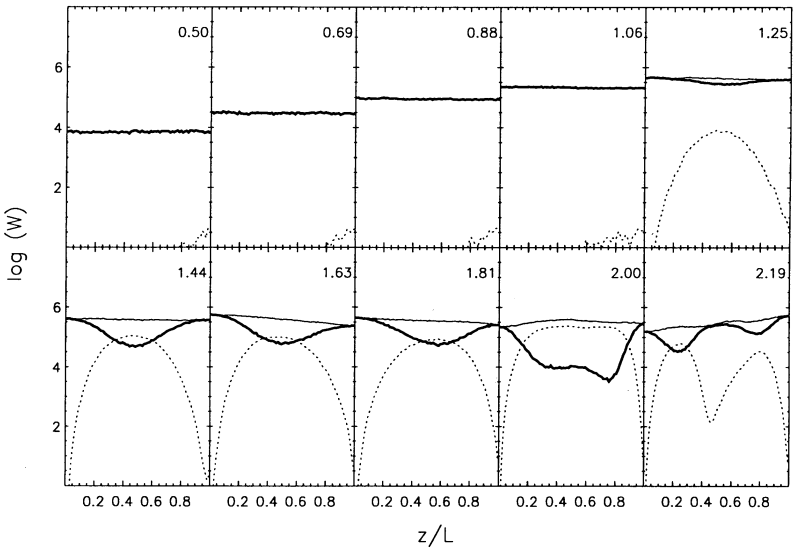

FIG. 4.—Total magnetic energy (*solid line*) as a function of z at different times (labeled). Horizontal curves correspond to force-free equilibria. The dotted curves correspond to total kinetic energy.

By the time the growth saturates, the spatial pattern is dominated by a new cell structure, which is now a combination of the three interacting Fourier modes. To see how this pattern depends on z, in Figure 6 we show a surface of constant stream function (30% of the maximum) at $t = 1.13$. Near the center of the loop, the spatial structure is dominated by the pattern of elliptic cells shown in Figure 5, but as we move toward the upper boundary, it smoothly changes to the pattern of photospheric motions. Since the lower plate corresponds to $\varphi = 0$, the surface does not reach this boundary.

As a result of this nonlinear loss of equilibrium, we see the emergence of new patterns (corresponding to Fourier modes $\boldsymbol{k}_1$ and $\boldsymbol{k}_2$) in the coronal part of both the vector potential and stream function, which are totally unrelated to the pattern of

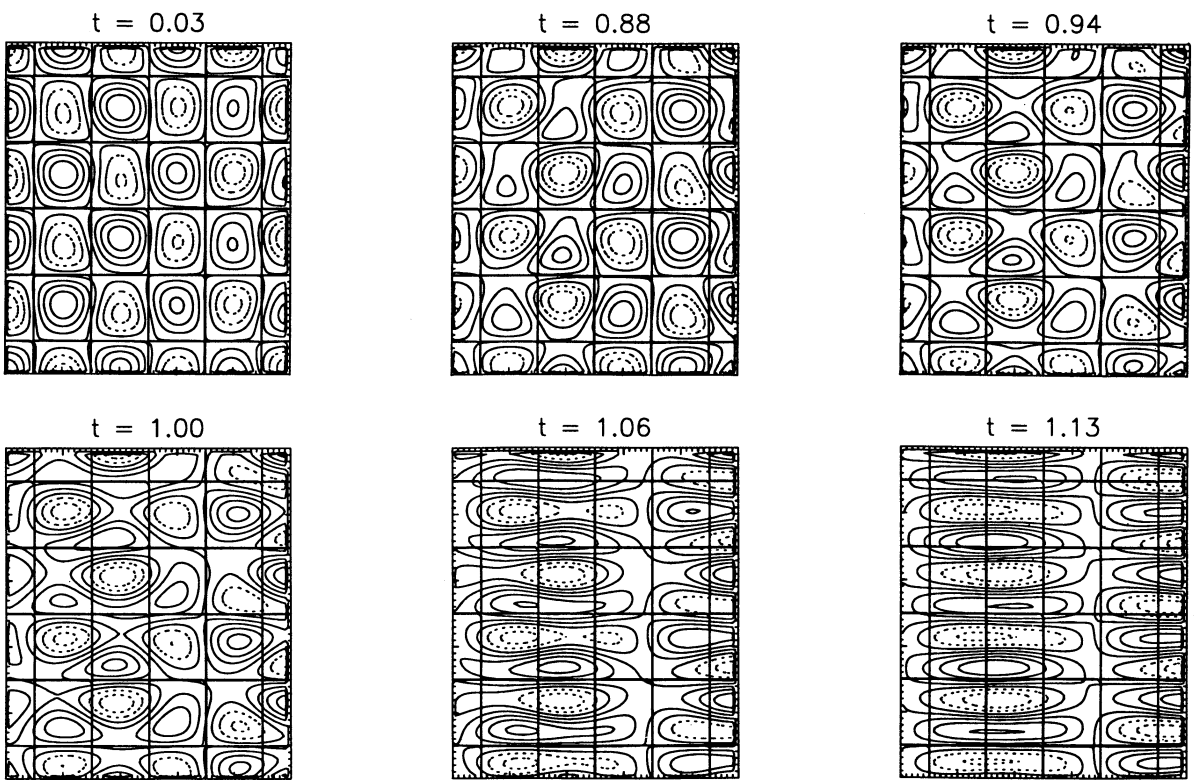

FIG. 5.—Time sequence of contour plots of the stream function at loop half-length ($z = \frac{1}{2}$ plane). The solid-line contours correspond to anti-clockwise motions (25%, 50%, and 75% of maximum), while the dotted contours correspond to clockwise trajectories. The square grid overlaid on all the plots corresponds to the cell pattern of photospheric motions.

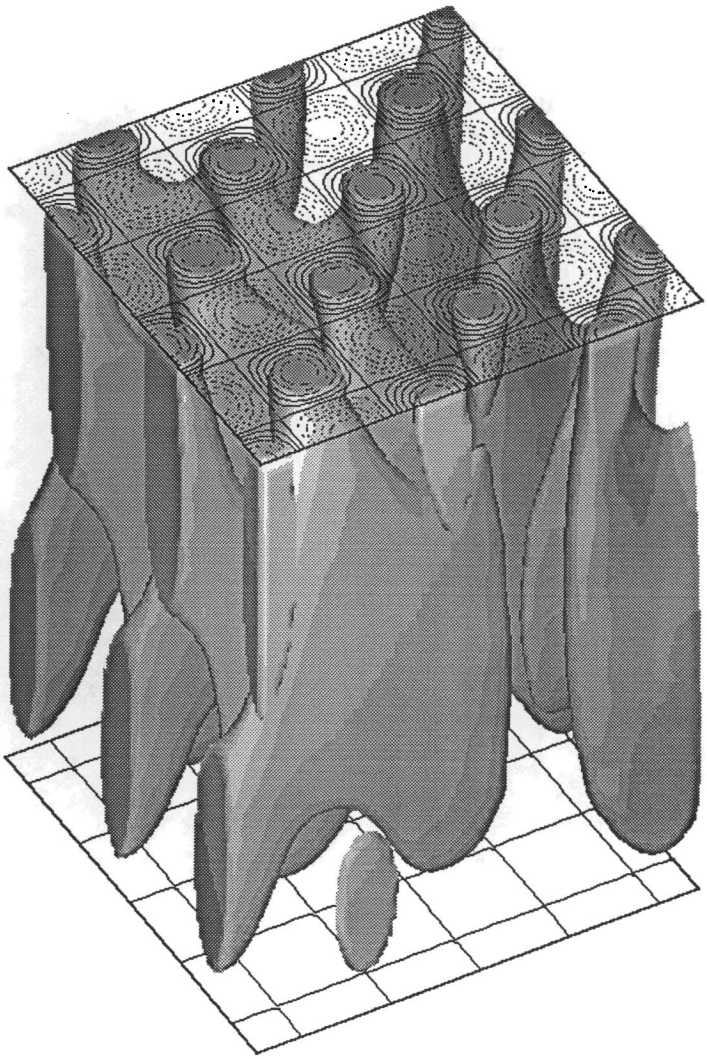

FIG. 6.—Surface of constant stream function (30% of maximum) at $t = 1.13$. Contour plots of the stream function at the upper boundary are also displayed for reference.

photospheric flow motions. In the next section we discuss the implications that loss of equilibrium in coronal loops might have for the heating of solar active regions.

6. DISCUSSION

Although it is widely believed that the energy necessary to heat the plasma confined in coronal loops comes from the dissipation of magnetic stresses, the precise dissipation mechanism is still a matter of debate. Current theories of magnetic coronal heating can be grouped into two categories: those proposing dissipation of MHD waves, and those which rely on the dissipation of DC currents. Wave heating is negligible for a spatially uniform coronal loop, but the dissipation rate can be increased considerably in the presence of inhomogeneities in the magnetic field (Heyvaerts & Priest 1983; see also Similon & Sudan 1989). On the other hand, the dissipation rate of large-scale DC currents is also negligible, and therefore the spatial distribution of electric currents has to be highly structured if Joule heating is assumed to be the dissipation mechanism (Parker 1983; van Ballegooijen 1986; Mikić et al. 1989). Either way, the development of small-scale spatial structure appears as a key ingredient in almost any current theory of coronal heating.

The generation of spatial structure in coronal loops is the result of nonlinearities in the corresponding dynamic equations. If we assume for a moment that the dynamics of a coronal loop can be described by the linearized RMHD equations, we find that the only spatial patterns that appear in the coronal part of the loop are those which are present in the photospheric flow. The role of nonlinearities is to make the different normal modes of the system to interact with one another, and eventually excite new modes, which do not receive direct excitation from the photospheric boundary motions.

In this paper we study the generation of new spatial structure, using a very simple model to simulate a coronal loop driven by footpoint motions. We use a truncated version of three Fourier modes of the reduced MHD (RMHD) equations, with only one of these modes being externally driven by a stationary flow of footpoint motions. The dynamic evolution of this model can be separated into three different stages:

1. The initial effect of the footpoint motions is simply to twist the magnetic fieldlines in such a way that they map the spatial pattern imposed at the photospheric boundaries. This first stage of the evolution can be described as a sequence of slowly changing force-free equilibria. The dynamics is completely dominated by the externally driven mode and the only relevant timescale is the photospheric turnover time.

2. On a timescale on the order of one turnover time, the corona can no longer evolve while remaining close to a quasi-static equilibrium. After the force-free equilibrium is lost, the energy of the nondriven modes grows like $W_{1+2} \approx \exp\,[(t/\tau_{\rm rise})^2]$, at the expense of the externally driven mode. This loss of equilibrium involves the emergence out of the noise level of new spatial structure in the interior of the loop, represented in our simple model by the superposition of two new Fourier modes.

3. The last stage in the evolution corresponds to the saturation of the growth of the new modes. In the results shown in Figures 2 and 3, the total energy seems to settle at an approximately constant level, implying that the corona stops absorbing energy from the photosphere. However, the three-mode approximation breaks down before the saturation is complete, so all we can state with certainty is that the new modes grow to a significant level before they saturate.

Note that even though we have concentrated our analysis on the most rapidly growing triad, other triads are simultaneously undergoing loss of equilibrium, as we show in Figure 1. Therefore we do not expect our results to be directly comparable to observations of the dynamics of coronal loops. The aim of the present paper is rather to point out the existence and efficiency of such nonequilibrium behavior in generating new spatial structure in the interior of coronal loops. As predicted by Parker (1972), loss of force-free equilibrium can be initiated by photospheric motions, and the resulting dynamic evolution can efficiently generate finer-scale structure in the corona. The elementary processes studied here can be regarded as part of a much more complex dynamical evolution.

7. CONCLUSIONS

If coronal loops are heated by the ohmic dissipation of currents produced by photospheric convective motions, the for-

mation of fine-scale structure is necessary to achieve the dissipation rate required to heat the corona. Such structures may be formed as a direct consequence of the turbulent nature of photospheric convection, as a result of magnetohydrodynamic instability in the corona, or as a result of "loss of equilibrium" which forces dynamic evolution away from a near force-free state.

We have demonstrated, in a very simple idealized system, the dynamic loss of equilibrium proposed by Parker (1972) as a means of dissipation of free magnetic energy. The rapid evolution away from force-free equilibrium occurs on a timescale which is the geometric mean of the Alfvén propagation time along the loop, and the photospheric turn-over time.

The growth of new modes produces finer scale structure, and a sizable fraction of the energy pumped into the corona by photospheric motions is transferred to the new modes. Although the extent of fine-scale structure is severely restricted in our simple three-mode model, we envision the elementary processes studied here as part of a much complex dynamical evolution.

D. G. expresses his gratitude to the organizers and participants of the Stanford Workshop on Coronal Heating (1992 February), because the basic ideas for the present paper were born after very fruitful discussions during that meeting. This work was supported by NSF grants ATM-9311937 and INT-9302098 to the University of Hawaii, by NSF grant ATM-9110514 to the Smithsonian Astrophysical Observatory, and by CONICET grant 3451/92 to IAFE.

REFERENCES

Golub, L., et al. 1990, Nature, 344, 842
Gómez, D. O. 1990, Fund. Cosmic Phys., 14, 131
Heyvaerts, J., & Priest, E. R. 1983, A&A, 137, 63
Longcope, D. W., & Sudan, R. N. 1991, Phys. Fluids, B4, 2277
———. 1992, ApJ, 384, 305
Mikić, Z., Schnack, D. D., & van Hoven, G. 1989, ApJ, 338, 1148
Narain, U., & Ulmschneider, P. 1990, Space Sci. Rev., 54, 377
Parker, E. N. 1972, ApJ, 174, 499
———. 1983, ApJ, 264, 642
Similon, P. L., & Sudan, R. N. 1989, ApJ, 336, 442
Segur, H. 1984, Contemporary Mathematics, 28, 281
Strauss, H. R. 1976, Phys. Fluids, 19, 134
van Ballegooijen, A. 1985, ApJ, 298, 421
———. 1986, ApJ, 311, 1001
Vaiana, G., & Rosner, R. 1978, ARA&A, 16, 393
Zakharov, V. E., L'vov, V. S., & Falkovich, G. 1992, Kolmogorov Spectra of Turbulence, Vol. 1 (Berlin: Springer), 1